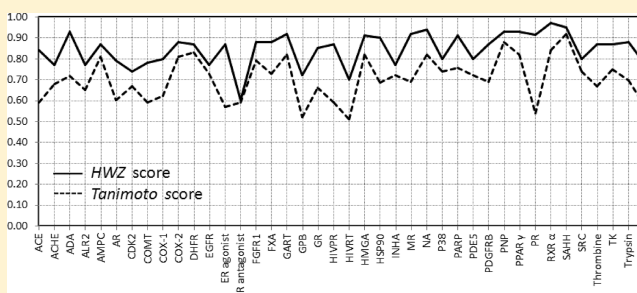


Ligand-Based Virtual Screening Approach Using a New Scoring Function

Adel Hamza,^{†,§} Ning-Ning Wei,^{†,‡,§} and Chang-Guo Zhan^{*,†}[†]Department of Pharmaceutical Sciences, College of Pharmacy, University of Kentucky, 789 South Limestone Street, Lexington, Kentucky 40536, United States[‡]School of Life Science and Biotechnology, Dalian University of Technology, No. 2 Linggong Road, Ganjingzi District, Dalian, Liaoning 116024, China

Supporting Information

ABSTRACT: In this study, we aimed to develop a new ligand-based virtual screening approach using an effective shape-overlapping procedure and a more robust scoring function (denoted by the HWZ score for convenience). The HWZ score-based virtual screening approach was tested against the compounds for 40 protein targets available in the Database of Useful Decoys (DUD; dud.docking.org/jahn/), and the virtual screening performance was evaluated in terms of the area under the receiver operator characteristic (ROC) curve (AUC), enrichment factor (EF), and hit rate (HR), demonstrating an improved overall performance compared to other popularly used approaches examined. In particular, the HWZ score-based virtual screening led to an average AUC value of 0.84 ± 0.02 (95% confidence interval) for the 40 targets. The average HR values at the top 1% and 10% of the active compounds for the 40 targets were $46.3\% \pm 6.7\%$ and $59.2\% \pm 4.7\%$, respectively. In addition, the performance of the HWZ score-based virtual screening approach is less sensitive to the choice of the target.



INTRODUCTION

Virtual screening approaches have been widely used in drug discovery processes for lead identification, lead optimization, and scaffold hopping. They provide an inexpensive and fast alternative to high-throughput screening for discovering new drugs.¹ There are two broad categories of computational techniques for virtual screening: (1) ligand-based drug design (e.g., ligand similarity) and (2) structure-based drug design (ligand docking) methods. The ligand similarity methods capitalize on the fact that ligands similar to an active ligand are more likely to be active than random ligands, whereas protein–ligand docking attempts to use the three-dimensional (3D) protein structure of the target protein to predict the binding modes and affinities of ligands to the target.

Ligand-based virtual screening methods use the information present in known active ligands rather than the structure of a target protein for both lead identification and optimization. Ligand-based methods are the only chosen when no 3D structure of the target protein is available. This is typically the case, for example, with G-protein-coupled receptor (GPCR) targets² or protein structures resolved in the apo form.³ In practice, without knowing the protein structure for the target of interest, one often knows that a set of ligands are active against the target of interest. As such, ligand-based virtual approaches can be employed, i.e. finding new ligands by evaluating the *similarity* between candidate ligands and the known active compounds.⁴ By using a ligand-based method, the known active compounds are collected in

order to select a query for virtual screening or alignment in ligand-based design.

A ligand-based computational method involves two essential elements: an efficient similarity measure and a reliable scoring method. In addition, the computational method should be able to screen a large number of potential ligands with reasonable accuracy and speed.

Thus, the similarity measures consist of geometrical information of arbitrary objects defined on the structures. The type of an object varies between different methods and can be classified into three types: pharmacophores, molecular shapes, and molecular fields. Pharmacophore-based methods generate patterns of distances between predefined molecular properties like aromatic systems or hydrogen-bond acceptors/donors⁵ and calculate the similarity value through a comparison of the corresponding patterns. Molecular shape approaches try to maximize the overlap of shapes and determine a similarity value based on the shape overlap. Ballester et al. introduced a nonsuperposition comparison algorithm for molecular shapes, called ultrafast shape recognition, and applied it to virtual screening experiments.⁶

A scoring method for ligand-based screening should effectively discriminate active compounds from the inactive ones during the ranking phase and can be used to efficiently

Received: December 21, 2011

Published: April 9, 2012

identify a small number of active compounds from a library including a large number of inactive compounds. See ref 7 for reviews of molecular similarity methods.

At present, the highly optimized screening platform ROCS (Rapid Overlay of Chemical Structures)⁸ (OpenEye Inc.) is considered as the industry standard for ligand shape-based virtual screening. It uses 3D Gaussian functions to describe the shape of query structures and to screen databases in search of molecular structures with similar shapes.^{8c} It is well-known that ROCS performance is highly dependent on the selection of query molecule.⁹ On the other hand, the current literature suggests that virtual screening performance of ROCS is essentially unaffected by choice of the conformation of a given query compound.^{9,10}

The available range of other shape-based screening tools and algorithms includes the algorithm Cat-Shape as implemented in CATALYST (Accelrys: San Diego),¹¹ the phase-Shape module as implemented in the Schrödinger software suite (Schrödinger, LLC), PARASHIFT,¹² Hex,¹³ ShaEP,¹⁴ and the USR (ultrafast shape recognition) algorithms.¹⁵ Putta and Beroza provided an excellent review¹⁶ on shape-based screening methods, alignment procedures, and the challenges. However, the performances of these software packages are often inconsistent across different databases and queries.¹⁴ In their recent work, Hawkins et al.¹⁰ pointed out that while docking usually suffers from a high false positive rate (i.e., inactive compounds are sometime identified as active compounds) the problem of shape-based screening is mainly its inferior false negative rate (i.e., a low score is incorrectly assigned to an active compound).¹⁷

Although the field of virtual screening may be maturing¹⁸ and many accurate methods have been proposed, the promise of the virtual compound library¹⁹ to rapidly increase the number of candidate ligands demands further improvement in terms of the computational efficiency of similarity measure algorithms and the scoring function.

The basic assumption of shape-based similarity screening is that molecules of shape and chemistry comparable to a known active compound (query structure) have a significant probability of also showing activity. Therefore, active ligands with shape differing from the query structure (which has been known to be active) are likely to be missed during virtual screening. For this purpose, it is necessary to continue the search for novel ligand-based strategy with the ability to identify more potent ligands of a drug target.

Despite many reports of successful applications of the ligand shape-based virtual screening methods, serious issues remain unsolved. For example, the shape (volume) based screening tools in some cases still cannot reliably identify the active ligands in the early stage of the database screening.²⁰ More importantly, the screening performance measured by the area under the receiver operator characteristic (ROC) curve (AUC) is for some targets equivalent to the random identification of active ligands from the database.^{14,20a} Indeed, Vainio et al.¹⁴ have compared the performance of the ShaEP and ROCS programs using the 40 targets available in the Database of Useful Decoys (DUD) (<http://dud.docking.org/>)²¹ and found that AUC was below 0.5 (an AUC value representing a failed screening) for nine targets screened using ShaEP and five targets screened using ROCS. In most of the cases, the ligand shape (volume) based virtual screening methods use the Tanimoto scoring function²² or a similar one²³ for ranking ligands, whereas a more sophisticated scoring function has been defined in the ROCS program in which both shape and a color

force field are used for optimization of the shape (volume) overlap.²⁴

In this report, we present a novel ligand-based virtual screening approach using an effective and efficient ligand similarity algorithm including an effective shape-overlapping procedure and a more robust scoring function. The novel ligand-based virtual screening approach has been tested against the 40 targets available in the DUD database²¹ in comparison with the performance of existing standard methods reported in literature, demonstrating the effectiveness of the ligand-based virtual screening approach.

METHODS

General Strategy. Unlike other ligand-based shape-overlapping methods, the main feature of our approach is to first find the finest starting superposition of the candidate structure (B from a database) with the query (A), which might result in an optimal and fast shape-density overlap convergence.

In the first step, a list of chemical (functional) groups, e.g. cyclo-hexane, alkyl chain, and halogen substitution, are identified for both the query (named List^A) and each candidate structure (named List^B). Subsequently, if the chemical groups of the List^B are not present in the List^A, the chemical groups will be removed from the candidate structure. If the List^B is entirely distinct from the List^A, the complete candidate structure will be preserved. This process is realized for each candidate structure in the database and a new database is built with “reduced” candidate structures (Figure S1 in the Supporting Information (SI)).

Shape-Overlapping Procedure. The shape overlapping procedure in our algorithm begins by overlapping the center of mass of the *reduced candidate structure* (molecule B) with that of the query structure and, then, aligning their principal moments of inertia.

This strategy allows us to explore the whole 3D space with a minimum number of iterations throughout the shape overlapping and optimization procedures and, thus, is expected to produce less false-positive overlaps. Moreover, this approach can significantly reduce the CPU time required for the shape overlapping process. Subsequently, the candidate ligand (molecule B) is replaced by its full structure. Then, the molecule B is moved (translation and rotation) as a rigid body to produce a quasi-optimal shape-density overlap V_{AB} with the query structure. Finally, the position and the orientation of molecule B are refined with respect to the rigid-body translations and rotations of the coordinates using the steepest descent method.²⁵ The optimized pose of molecule B, which should have an optimal shape-density overlap V_{AB} , is then compared to the poses already in a temporary file to determine if the candidate pose should be accepted, and the temporary file is updated accordingly. An efficient algorithm based on quaternions²⁶ is used to compute the rotations of the structure coordinates around the axis of the coordinate system.

Scoring of the Shape-Overlapped Structure. Currently, a major weakness of ligand-based screening approach, i.e. the inability to consistently identify true positives (active compounds), is likely due to the imprecise scoring methods. It has been known that the use of the Tanimoto scoring function²² or a similar one²³ was inadequate for some targets. For example, the recent screening test using the DUD database realized by Vainio et al. and Kirchmair et al. demonstrated that the enrichment factor and AUC metrics were largely dependent on the screened system and even failed for some targets.^{14,20a}

A crucial issue is the relative scores of a candidate ligand with a size larger than the query ligand and a candidate ligand with a size smaller than the query ligand. To demonstrate the feature of the Tanimoto scoring function, we have illustrated in Figure 1

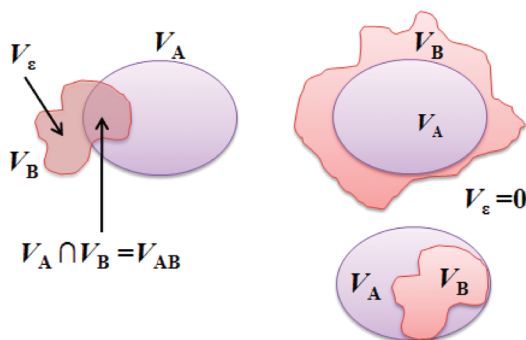


Figure 1. Classical representation of the shape-based shape similarity between two molecules A and B (left). Representation of the optimal shape overlap V_{AB} , i.e. $V_\epsilon = 0$, when $V_B > V_A$ (top right) and $V_B < V_A$ (bottom right).

the concept of density/volume-based shape similarity between two structures (for the query ligand A and candidate ligand B); each is represented by a set of hard atomic spheres. The superimposition of ligands A with B is scored according to the shape-density overlap V_{AB} between the query (ligand A) with volume V_A and testing structure (B) with volume V_B . The commonly occupied volume $V_{A \cap B}$ is normalized by the total volume $V_{A \cup B}$ to arrive at a Tanimoto-like shape similarity:

$$T = V_{A \cap B} / V_{A \cup B}$$

$$T = \frac{V_{AB}}{V_A + V_B - V_{AB}} \quad (1a)$$

It is interesting to note the following two possible conditions:

- (1) When $V_B < V_A$ the volume overlap between ligands A and B is $V_{AB} = V_B - V_\epsilon$ (see Figure 1), in which V_ϵ represents the residual volume of ligand B which does not overlap with the query ligand A. Under this condition, eq 1a becomes

$$T^{(1)} = (V_B - V_\epsilon) / [V_A + V_B - (V_B - V_\epsilon)]$$

$$T^{(1)} = (V_B - V_\epsilon) / (V_A + V_\epsilon) \quad (1b)$$

Specially, when $V_\epsilon = 0$, eq 1b becomes

$$T^{(1)} = V_B / V_A \quad (1c)$$

- (2) Using the same notations, when $V_B > V_A$ and $V_\epsilon = 0$, eq 1a becomes

$$T^{(2)} = (V_A - V_\epsilon) / [V_A + V_B - (V_A - V_\epsilon)]$$

$$T^{(2)} = V_A / V_B \quad (1d)$$

Equations 1c and 1d clearly reveal that, under these extreme conditions, the ranking of the candidate ligands (B) is determined by two inhomogeneous criteria, i.e. eqs 1c and 1d, according to the Tanimoto scoring function. By using eqs 1c and 1d, one can obtain the perfect score ($T = 1$) for ligand B when $V_B = V_A$. When $V_B < V_A$ and the volume difference is xV_A , we have $V_B = (1 - x)V_A$ and eq 1c gives

$$T^{(1)} = 1 - x \quad (1e)$$

When $V_B > V_A$ and the volume difference is xV_A , we have $V_B = (1 + x)V_A$ and eq 1d gives

$$T^{(2)} = 1 / (1 + x) \quad (1f)$$

Clearly, $T^{(2)}$ in eq 1f is always bigger than $T^{(1)}$ in eq 1e for a given x value, as depicted in Figure 2A. So, the Tanimoto

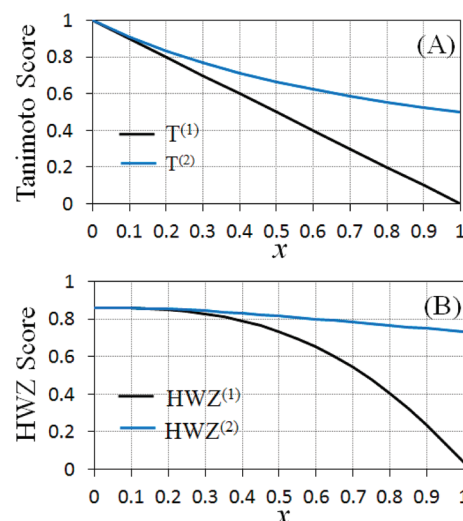


Figure 2. (A) Plots of the Tanimoto score versus x in eqs 1e and 1f when $V_\epsilon = 0$ and $V_B = (1 \pm x)V_A$. (B) Plots of the corresponding HWZ score versus x when $V_\epsilon = 0$ and $V_B = (1 \pm x)V_A$ in eqs 2b and 2c.

scoring function always gives the advantage to the candidate ligands whose sizes are larger than the query ligand in comparison with the candidate ligands whose sizes are smaller than the query ligand. In other words, the Tanimoto scoring function might bias to the candidate ligands whose sizes are larger than the query ligand.

We have developed a new scoring approach to solve the scoring function problem. Specifically, the candidate ligands are ranked according to a uniform scoring function, denoted by Hamza–Wei–Zhan (HWZ) score for convenience:

$$HWZ = \sum_{k=1}^N \left[a_k \left(\frac{V_{AB}}{V_A} \right)^k + b_k \left(\frac{V_{AB}}{V_B} \right)^k + c_k \left(\frac{V_{AB}}{V_A + V_B} \right)^k \right] \quad (2a)$$

in which the coefficients a_k , b_k , and c_k have been calibrated through extensive training and testing against 16 drug targets collected in “The Binding Database” (www.bindingdb.org/bind/index.jsp). See below for the choice of N .

To compare the feature of the HWZ scoring function with that of the Tanimoto scoring function, we also used the aforementioned extreme conditions and notations to analyze

Table 1. Calibrated Coefficients of HWZ Scoring Function (with $N = 3$)

| k | a_k | b_k | c_k |
|-----|-------|-------|-------|
| 1 | 0.02 | 0.02 | 0.98 |
| 2 | 0 | 0 | 1.09 |
| 3 | 0 | 0 | −2.98 |

Table 2. Areas under the ROC curves ($\langle AUC \rangle$) for the 40 DUD Targets (N_{target}) Using the HWZ and Tanimoto Scoring Functions and the Previously Published Results Using the ROCS and ShaEP Programs^a

| Range of $\langle AUC \rangle$ | $0 \leq AUC \leq 1$ | | $0.8 \leq AUC \leq 1$ | | $0.6 \leq AUC < 0.8$ | | $0.6 < AUC$ | |
|--------------------------------|-----------------------|---------------------|-----------------------|---------------------|-----------------------|---------------------|-----------------------|---------------------|
| | $\langle AUC \rangle$ | N_{target} | $\langle AUC \rangle$ | N_{target} | $\langle AUC \rangle$ | N_{target} | $\langle AUC \rangle$ | N_{target} |
| this work–HWZ | 0.84 ± 0.02 | 40 | 0.88 ± 0.02 | 29 (72%) | 0.74 ± 0.01 | 11 (28%) | | 0 |
| this work–Tanimoto | 0.70 ± 0.03 | 40 | 0.84 ± 0.02 | 10 (25%) | 0.70 ± 0.02 | 21 (52%) | 0.59 ± 0.02 | 9 (23%) |
| Kirchmair–ROCS ^b | 0.73 ± 0.06 | 40 | 0.92 ± 0.02 | 17 (42%) | 0.72 ± 0.03 | 11 (28%) | 0.47 ± 0.05 | 12 (30%) |
| Vainio–ROCS ^c | 0.69 ± 0.05 | 40 | 0.90 ± 0.04 | 12 (30%) | 0.70 ± 0.03 | 14 (35%) | 0.50 ± 0.03 | 14 (35%) |
| Vainio–ShaEP ^c | 0.64 ± 0.05 | 40 | 0.86 ± 0.01 | 8 (20%) | 0.70 ± 0.03 | 16 (40%) | 0.47 ± 0.05 | 16 (40%) |

^aROCS uses the Combo Scoring function (Shape-Tanimoto and Scaled Color score), and ShaEP uses the Hodgkin similarity index. ^bData from ref 20a. ^cData from ref 14.

the HWZ function. Specifically, when $V_B < V_A$ and $V_E = 0$, eq 2a gives

$$HWZ^{(1)} = \sum_{k=1}^N \left[a_k \left(\frac{V_B}{V_A} \right)^k + b_k \left(\frac{V_B}{V_B} \right)^k + c_k \left(\frac{V_B}{V_A + V_B} \right)^k \right] \quad (2b)$$

When $V_B > V_A$ and $V_E = 0$, eq 2a gives

$$HWZ^{(2)} = \sum_{k=1}^N \left[a_k \left(\frac{V_A}{V_A} \right)^k + b_k \left(\frac{V_A}{V_B} \right)^k + c_k \left(\frac{V_A}{V_A + V_B} \right)^k \right] \quad (2c)$$

As depicted in Figure 2B, the HWZ scoring functions does not significantly bias to the candidate ligands whose sizes are larger than the query ligand when $x < 0.3$. So, it is interesting to examine the performance of this new scoring function in comparison with the Tanimoto (T) scoring function.²²

Calibration of the HWZ Scoring Function. The empirical parameters (a_k , b_k , and c_k) in the HWZ scoring function represented by eq 2a were determined by iteratively adjusting the parameter values based on the extensive, repeated training and testing tests against 16 targets (listed in SI Table S1) with a total of 2784 active ligands (see SI Table S2) collected in The Binding Database (www.bindingdb.org/bind/index.jsp). The training and testing with each target included all of the active ligands available in the The Binding Database. For each target, the available active ligands were randomly partitioned into training set (50%) and testing set (50%). The random partition was repeated for five times, and the average results for the testing were taken. For each time, each of the 50% active ligands in the training set had an opportunity to be used as the query. For the training, the 50% active ligands in the training set were seeded into a decoy set to create a screening database for training. The decoy set consisted of 700 decoys that were selected randomly from the ZINC database (<http://zinc.docking.org/>). Similarly, the other 50% of active ligands in the testing set were also seeded into a decoy set (that consisted of 700 different decoys selected randomly from the ZINC database) to create a screening database for testing.

The screening database for training or testing was conformationally expanded by using OMEGA (OpenEye Scientific Software) with parameters as described before.²⁷ We note that 700 was an arbitrary number for a decoy set. The arbitrary number of 700 decoys representing the structural noise of the database was chosen due to a compromise between the accuracy of the computed parameters and the cumulative computing time. Our additional training and testing indicated that adding more decoys would not significantly change/improve the calibrated scoring function.

Table 3. Areas under the ROC Curves (AUC) for the 40 Targets in the DUD Database Based on the HWZ and Tanimoto Scoring Functions in Comparison with the Previously Published Data Using the ROCS Program

| target | HWZ score | Tanimoto score | ROCS ^a | ROCS ^b |
|----------------|-------------|----------------|-------------------|-------------------|
| ACE | 0.84 ± 0.04 | 0.59 ± 0.04 | 0.70 | 0.76 |
| ACHE | 0.77 ± 0.06 | 0.68 ± 0.06 | 0.77 | 0.75 |
| ADA | 0.93 ± 0.01 | 0.72 ± 0.01 | 0.86 | 0.85 |
| ALR2 | 0.77 ± 0.05 | 0.65 ± 0.05 | 0.57 | 0.52 |
| AMPC | 0.87 ± 0.06 | 0.81 ± 0.06 | 0.82 | 0.86 |
| AR | 0.79 ± 0.06 | 0.60 ± 0.06 | 0.79 | 0.48 |
| CDK2 | 0.74 ± 0.06 | 0.67 ± 0.06 | 0.68 | 0.61 |
| COMT | 0.78 ± 0.04 | 0.59 ± 0.04 | 0.32 | 0.39 |
| COX-1 | 0.80 ± 0.03 | 0.62 ± 0.03 | 0.53 | 0.54 |
| COX-2 | 0.88 ± 0.04 | 0.81 ± 0.04 | 0.93 | 0.68 |
| DHFR | 0.87 ± 0.01 | 0.83 ± 0.01 | 0.92 | 0.95 |
| EGFR | 0.77 ± 0.02 | 0.73 ± 0.02 | 0.95 | 0.62 |
| ER agonist | 0.87 ± 0.03 | 0.57 ± 0.03 | 0.94 | 0.92 |
| ER antagonist | 0.60 ± 0.01 | 0.59 ± 0.01 | 0.98 | 0.78 |
| FGFR1 | 0.88 ± 0.08 | 0.79 ± 0.08 | 0.49 | 0.57 |
| FXA | 0.88 ± 0.03 | 0.73 ± 0.03 | 0.39 | 0.52 |
| GART | 0.92 ± 0.04 | 0.82 ± 0.04 | 0.93 | 0.79 |
| GPB | 0.72 ± 0.03 | 0.52 ± 0.03 | 0.92 | 0.94 |
| GR | 0.85 ± 0.03 | 0.66 ± 0.03 | 0.79 | 0.73 |
| HIVPR | 0.87 ± 0.05 | 0.59 ± 0.05 | 0.56 | 0.55 |
| HIVRT | 0.70 ± 0.08 | 0.51 ± 0.08 | 0.66 | 0.62 |
| HMGA | 0.91 ± 0.02 | 0.82 ± 0.02 | 0.92 | 0.78 |
| HSP90 | 0.90 ± 0.06 | 0.69 ± 0.06 | 0.66 | 0.80 |
| INHA | 0.77 ± 0.05 | 0.72 ± 0.05 | 0.72 | 0.69 |
| MR | 0.92 ± 0.02 | 0.69 ± 0.02 | 0.87 | 0.82 |
| NA | 0.94 ± 0.01 | 0.82 ± 0.01 | 0.97 | 0.98 |
| P38 | 0.80 ± 0.09 | 0.74 ± 0.09 | 0.52 | 0.43 |
| PARP | 0.91 ± 0.08 | 0.76 ± 0.08 | 0.58 | 0.62 |
| PDES | 0.80 ± 0.05 | 0.72 ± 0.05 | 0.53 | 0.52 |
| PDGFRB | 0.87 ± 0.04 | 0.69 ± 0.04 | 0.34 | 0.40 |
| PNP | 0.93 ± 0.04 | 0.88 ± 0.04 | 0.91 | 0.90 |
| PPAR γ | 0.93 ± 0.04 | 0.82 ± 0.04 | 0.92 | 0.65 |
| PR | 0.92 ± 0.02 | 0.54 ± 0.02 | 0.67 | 0.53 |
| RXR α | 0.97 ± 0.01 | 0.84 ± 0.01 | 0.96 | 0.98 |
| SAHH | 0.95 ± 0.01 | 0.92 ± 0.01 | 0.97 | 0.99 |
| SRC | 0.80 ± 0.06 | 0.74 ± 0.06 | 0.38 | 0.47 |
| Thrombine | 0.87 ± 0.04 | 0.67 ± 0.04 | 0.66 | 0.57 |
| TK | 0.87 ± 0.04 | 0.75 ± 0.04 | 0.86 | 0.86 |
| Trypsin | 0.88 ± 0.06 | 0.70 ± 0.06 | 0.78 | 0.69 |
| VEGFR2 | 0.78 ± 0.06 | 0.58 ± 0.06 | 0.43 | 0.50 |
| average | 0.84 | 0.70 | 0.73 | 0.69 |
| 95% confidence | 0.02 | 0.03 | 0.06 | 0.02 |

^aData from ref 20a. ^bData from ref 14.

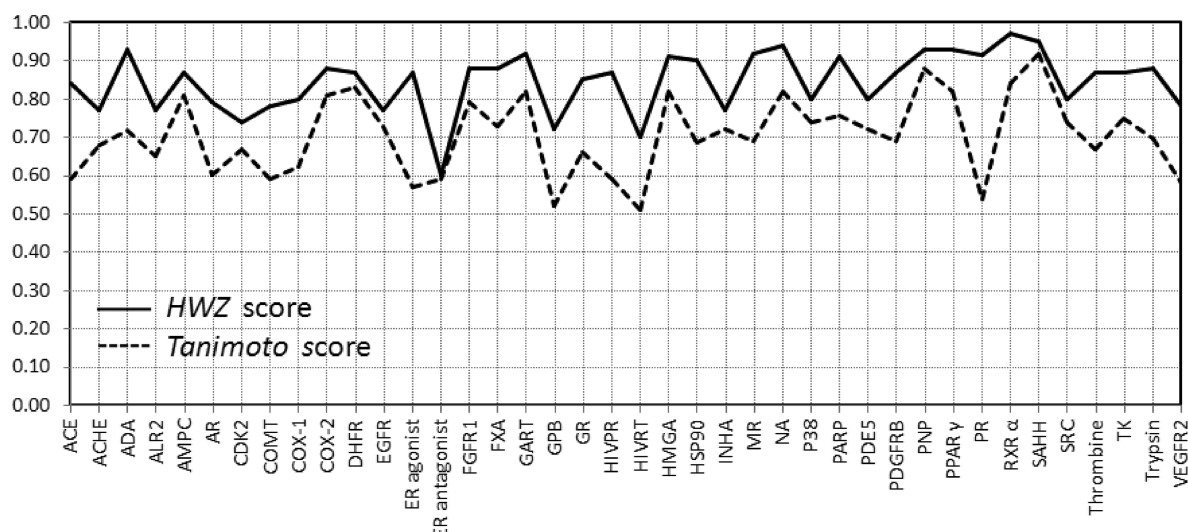


Figure 3. Area under the ROC curve (AUC) for the 40 targets in the DUD database, reflecting the performance of the ligand-based virtual screening using the HWZ and Tanimoto scoring functions.

Table 4. Comparison of the Areas under the ROC Curves (AUC) Obtained with HWZ Score and from Five Distinct Programs/Scoring Functions Using Nine DUD Targets^a

| target | HWZ score | NNscore 1.0 ^b | NNscore 2.0 ^b | AutoDock _{fast} ^b | AutoDock _{Rigorous} ^b | Vina ^b |
|-----------|-------------|--------------------------|--------------------------|---------------------------------------|---|-------------------|
| ACHE | 0.77 ± 0.06 | 0.55 | 0.57 | 0.48 | 0.53 | 0.67 |
| COX-2 | 0.88 ± 0.04 | 0.74 | 0.49 | 0.38 | 0.43 | 0.31 |
| DHFR | 0.87 ± 0.01 | 0.72 | 0.83 | 0.83 | 0.95 | 0.76 |
| EGFR | 0.77 ± 0.02 | 0.47 | 0.51 | 0.51 | 0.49 | 0.61 |
| FGFR1 | 0.88 ± 0.08 | 0.58 | 0.55 | 0.41 | 0.35 | 0.46 |
| FXA | 0.88 ± 0.03 | 0.76 | 0.52 | 0.44 | 0.47 | 0.63 |
| P38 | 0.80 ± 0.09 | 0.75 | 0.58 | 0.4 | 0.37 | 0.54 |
| PDGFRB | 0.87 ± 0.04 | 0.6 | 0.62 | 0.50 | 0.36 | 0.53 |
| SRC | 0.80 ± 0.06 | 0.58 | 0.63 | 0.65 | 0.58 | 0.69 |
| average | 0.83 | 0.64 | 0.59 | 0.51 | 0.50 | 0.58 |
| std. dev. | 0.05 | 0.10 | 0.10 | 0.15 | 0.18 | 0.14 |

^aThe highest AUC value for each target is highlighted in bold. ^bThe AUC values from ref 39.

For both the training and testing, the ligands were ranked according to the scoring function. The area under the ROC curve (AUC) metric was calculated for each query and the average value, $\langle \text{AUC} \rangle$, for the active ligands. The optimal parameter values of the HWZ scoring function were reached for the highest possible $\langle \text{AUC} \rangle$ value obtained from the testing on all of the 2784 active ligands for the 16 targets. Technically, we first calibrated the parameters a_k , b_k , and c_k against each of the 16 targets and obtained 16 different sets of parameter values. Then, we took the averages as the initial values to further optimize the parameter values and test the overall performance of the HWZ scoring function against all of the 16 targets.

Molecular Shape-Density Model. As suggested by Grant et al.,^{8a,28} it is reasonable to approximate the molecular electron density function simply as a superposition of atom-centered Gaussian functions. Thus, the molecular shape-density of a ligand is calculated using the Gaussian function, which uses a representation in which each atom i with coordinates $\mathbf{R}_i = (X_i, Y_i, Z_i)$ is given by a spherical Gaussian:

$$\rho_i(\mathbf{r}) = p_i \exp(-\alpha_i(\mathbf{r} - \mathbf{r}_i)^2) \text{ in which } \alpha_i = \pi \left(\frac{3p_i}{4\pi\sigma_i^3} \right)^{2/3} \quad (3)$$

The amplitude is set to $\rho_i = 2\sqrt{2}$, and the decay factor α_i is calculated from p_i and σ_i is the van der Waals radius of the atom i .²⁸ The molecular shape-density is the sum of all individual atomic densities. The molecular shape-density is given by

$$V_A = \sum_{i=0}^n \int d\mathbf{r} \rho_i(\mathbf{r}) \quad (4)$$

The shape-density overlap of two molecules A and B is defined as

$$\begin{aligned} V_{AB} &= \sum_{i \in A} \sum_{j \in B} \int d\mathbf{r} \rho_i(\mathbf{r}) \rho_j(\mathbf{r}) \\ &= \sum_{i \in A} \sum_{j \in B} p_i p_j \exp \left(-\frac{\alpha_i \alpha_j d_{ij}^2}{\alpha_i + \alpha_j} \right) \left(\frac{\pi}{\alpha_i + \alpha_j} \right)^{3/2} \end{aligned} \quad (5)$$

where i and j refer to atoms in molecules A and B, respectively, and d_{ij} is the distance between atoms i and j . In order to perform the superposition between a pair of molecules, the algorithm translates the molecular shape-density of the moving molecule (B) to that of the query structure (molecule A) and then searches for the rotation that minimizes the “distance” between the corresponding pairs of spherical Gaussian functions.

Validation. The above approach using the HWZ or Tanimoto scoring function has been coded in Fortran90 as a standalone module (denoted by SABRE, or *shape-approach-based routines enhanced*, for convenience of the use in our lab). The implementation has provided an opportunity for us to calibrate and validate the scoring function, i.e. eq 2a. The validation of our approach was based on an appropriate use of the DUD database²⁹ of annotated active compounds and decoys. The DUD is a publicly available virtual screening test database and is the second data set used by Cross et al.³⁰ It consists of 40 pharmaceutically relevant protein targets, each with a set of molecules known to be active against the protein target and many decoys. Currently, the DUD is considered as the industry standard for validation of docking and related protocols, and recently, it has also been applied to the evaluation of related structure-based and ligand-based virtual screening methods.^{31,21} The DUD was downloaded from Web site (http://dud.docking.org/jahn/DUD_LIB_VS_1.0.tar.gz in sdf file format).²¹

For our virtual screening tests against each target in the DUD database, the ratio of the number of decoys to the number of active ligands was fixed at ~ 36 , i.e. (number of decoys)/(number of active ligands) = ~ 36 , in order to be consistent with the ratio used in the previously published virtual screening tests.

To evaluate the effectiveness of the virtual screening approach, we first generated various molecular orientations and multiple conformations of each ligand (active or decoy) of the 40 targets in the DUD using OMEGA (OpenEye).³² OMEGA sampling is capable of selecting a ligand conformation similar to that of the targeted X-ray crystal structure by using an appropriate option (*default*) including a low-energy cutoff to discard high-energy conformations, a low root-mean-square deviation (rmsd) value below which two conformations are considered to be similar.³³ Atom typing, energy calculations, and geometry optimization in OMEGA were performed using the Merck Molecular Force Field (MMFF). The maximum allowed conformations per compound was set to 200, and the energy window (the value used to discard high-energy conformations) was set to 10 kcal/mol. The default values of the OMEGA program were used for other parameters.

Evaluation of the Virtual Screening Efficiency. For evaluating the effectiveness of a virtual screening of all compounds in a database against a given protein target, a popularly used and the simplest metric method is the enrichment at a given percentage of the database screened.³⁴ The enrichment factor (EF) is defined as

$$EF^{x\%} = \frac{\text{Hits}_{\text{selected}}^{x\%}/N_{\text{selected}}^{x\%}}{\text{Hits}_{\text{total}}/N_{\text{total}}} \quad (6)$$

where $\text{Hits}_{\text{selected}}^{x\%}$ is the number of hits (active ligands) found at top $x\%$ of the database screened, $N_{\text{selected}}^{x\%}$ is the number of compounds screened at top $x\%$ of the database, $\text{Hits}_{\text{total}}$ is the number of active ligands in entire database, and N_{total} is the number of compounds in entire database. The $EF^{x\%}$ metric relies on cutoffs made at various points through the ranking and so can be sensitive to small changes in ranking. A disadvantage of the EF is its high dependency on the ratio of active compounds of the database screened.³⁵ This obstacle makes the descriptor unsuitable for the direct comparison of performance investigations and screening runs that are based on test sets of different ratios between the active and inactive compounds. To avoid this problem and to appropriately compare the effectiveness of our approach with

Table 5. Enrichment Factor EF at Top 1%, 5%, and 10% Obtained from our HWZ Score-Based Virtual Screening in Comparison with the Data Published by Kirchmair et al.^{20a} Using the ROCS Program

| target | EF 1% | | EF 5% | | EF 10% | |
|----------------|-----------|-------------------|-----------|-------------------|-----------|-------------------|
| | HWZ score | ROCS ^a | HWZ score | ROCS ^a | HWZ score | ROCS ^a |
| ACE | 18.7 | 27.7 | 7.0 | 8.2 | 3.1 | 4.7 |
| ACHE | 27.1 | 26.8 | 8.5 | 12.6 | 5.8 | 7.4 |
| ADA | 29.1 | 13.8 | 13.5 | 3.5 | 6.4 | 3.9 |
| ALR2 | 15.6 | 8.1 | 6.9 | 3.1 | 4.9 | 3.1 |
| AMPC | 27.3 | 35.9 | 11.0 | 13.6 | 5.2 | 7.2 |
| AR | 26.1 | 27.0 | 7.2 | 9.5 | 5.1 | 5.1 |
| CDK2 | 18.7 | 26.4 | 5.1 | 6.4 | 4.0 | 4.0 |
| COMT | 16.3 | 30.1 | 8.3 | 5.5 | 4.6 | 2.7 |
| COX-1 | 7.6 | 17.5 | 4.8 | 5.7 | 4.1 | 2.8 |
| COX-2 | 8.9 | 35.7 | 4.0 | 17.1 | 7.2 | 8.7 |
| DHFR | 29.2 | 33.5 | 15.5 | 14.0 | 8.9 | 8.2 |
| EGFR | 30.5 | 33.0 | 11.8 | 16.9 | 5.3 | 8.9 |
| ER agonist | 25.1 | 27.1 | 12.1 | 16.1 | 6.2 | 9.0 |
| ER antagonist | 21.0 | 5.3 | 8.6 | 15.0 | 5.6 | 9.8 |
| FGFR1 | 21.7 | 0.0 | 11.2 | 2.4 | 5.5 | 2.0 |
| FXA | 33.5 | 4.3 | 14.2 | 1.0 | 6.8 | 0.8 |
| GART | 12.3 | 0.0 | 12.9 | 3.9 | 8.1 | 5.7 |
| GPB | 17.6 | 36.6 | 7.8 | 14.6 | 5.2 | 8.1 |
| GR | 23.2 | 15.8 | 7.9 | 5.2 | 4.5 | 5.7 |
| HIVPR | 28.1 | 5.8 | 7.5 | 2.3 | 5.6 | 1.5 |
| HIVRT | 19.1 | 21.1 | 5.4 | 4.6 | 4.2 | 2.5 |
| HMGA | 30.2 | 36.5 | 16.8 | 15.6 | 7.9 | 8.3 |
| HSP90 | 33.1 | 36.8 | 10.5 | 9.2 | 5.7 | 4.6 |
| INHA | 7.7 | 36.7 | 6.7 | 9.9 | 4.7 | 5.1 |
| MR | 32.2 | 36.7 | 15.1 | 16.3 | 8.4 | 8.0 |
| NA | 26.8 | 32.3 | 13.1 | 18.5 | 7.6 | 9.6 |
| P38 | 24.6 | 10.2 | 10.7 | 2.8 | 5.1 | 2.0 |
| PARP | 34.0 | 3.1 | 14.3 | 3.1 | 6.6 | 3.7 |
| PDE5 | 22.4 | 16.2 | 11.1 | 4.0 | 5.6 | 2.4 |
| PDGFRB | 12.5 | 7.7 | 7.2 | 1.7 | 4.4 | 1.1 |
| PNP | 29.6 | 20.2 | 14.8 | 16.9 | 7.4 | 9.3 |
| PPAR γ | 41.0 | 21.6 | 15.7 | 15.8 | 6.5 | 8.3 |
| PR | 32.1 | 16.4 | 12.4 | 3.0 | 7.1 | 2.6 |
| RXR α | 36.3 | 26.0 | 18.5 | 17.2 | 9.2 | 8.6 |
| SAHH | 26.5 | 26.3 | 16.1 | 14.7 | 8.8 | 9.4 |
| SRC | 18.9 | 2.0 | 9.7 | 1.6 | 5.0 | 1.0 |
| Thrombine | 21.2 | 1.8 | 7.3 | 1.1 | 5.6 | 0.7 |
| TK | 19.7 | 13.7 | 8.7 | 4.6 | 4.9 | 6.0 |
| Trypsin | 32.5 | 0.0 | 12.7 | 0.0 | 5.9 | 2.8 |
| VEGFR2 | 8.8 | 0.0 | 5.0 | 0.3 | 3.9 | 0.4 |
| average | 23.7 | 19.4 | 10.4 | 8.4 | 5.9 | 5.1 |
| 95% confidence | 2.6 | 4.0 | 1.2 | 1.9 | 0.5 | 0.9 |

^aData from ref 20a.

other well-known ligand-based approaches, we have also compared the obtained actual $EF^{x\%}$ value (denoted by $EF_{\text{actual}}^{x\%}$) with the desirable ideal $EF^{x\%}$ value (denoted by $EF_{\text{ideal}}^{x\%}$) for each of the 40 targets in the DUD database. This defines another way that portrays the effectiveness at fixed percentages through the database, named the hit rate ($HR^{x\%}$) corresponding to the ratio of the known hits:³⁶

$$HR^{x\%} = \frac{EF_{\text{actual}}^{x\%}}{EF_{\text{ideal}}^{x\%}} \times 100 \quad (7)$$

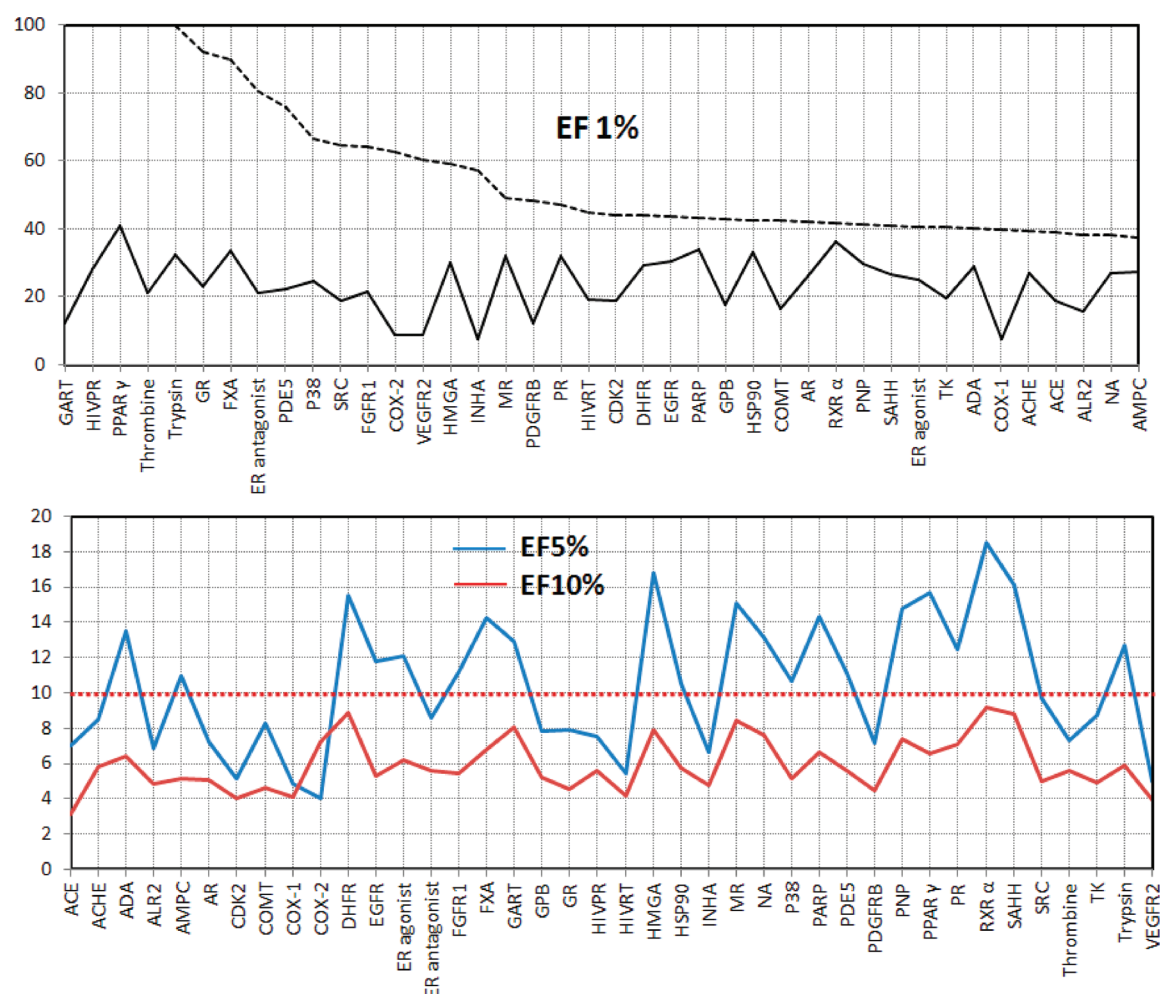


Figure 4. (top) Enrichment factor (EF) values at top 1%, 5%, and 10% obtained from the HWZ score-based virtual screening. We have also reported the $EF_{ideal}^{x\%}$ values for comparison (dashed lines). For clarity, the enrichment factor $EF^{1\%}$ was sorted from the highest $EF_{ideal}^{1\%}$ to the lowest one. (bottom) Ideal enrichment factor at top 1% and 5%: 10 (red dashed line) and 20, respectively.

Table 6. Enrichment Factor at Top 1% and 10% Obtained with HWZ Score and Several Distinct Programs Corresponding to Ligand/Structural-Based Virtual Screenings^a

| target | HWZ score | | Suflex-sim ^b | | FlexS ^b | | ICMsim ^b | |
|--------------|-----------|-----------|-------------------------|------|--------------------|-------------|---------------------|-------------|
| | 1% | 10% | 1% | 10% | 1% | 10% | 1% | 10% |
| ADA | 29.1 | <u>64</u> | 5.1 | 23.1 | 15.4 | 30.8 | 10.3 | 28.2 |
| CDK2 | 18.7 | <u>40</u> | 2.8 | 8.3 | 5.6 | 11.1 | 9.7 | 30.6 |
| DHFR | 29.2 | <u>89</u> | 4.9 | 25.6 | 8.0 | 27.8 | 20.2 | 80.7 |
| FXA | 33.3 | <u>68</u> | 1.4 | 2.7 | 5.5 | 19.9 | 11.6 | 46.6 |
| HIVRT | 19.1 | 42 | 9.3 | 18.6 | 27.9 | <u>58.1</u> | 18.6 | 39.5 |
| NA | 26.8 | <u>76</u> | 16.3 | 55.1 | 20.4 | 69.4 | 16.3 | 73.5 |
| P38 | 24.6 | <u>51</u> | 9.0 | 21.1 | 12.6 | 26.2 | 11.2 | 17.8 |
| thrombin | 21.2 | 56 | 1.4 | 15.3 | 2.8 | 12.5 | 2.8 | <u>76.4</u> |
| TK | 19.7 | 49 | 22.7 | 50 | 9.1 | 54.5 | 22.7 | <u>63.6</u> |
| trypsin | 32.5 | 59 | 0 | 59.2 | 18.4 | 18.4 | 10.2 | <u>95.9</u> |
| average | 25.4 | 59.4 | 7.3 | 27.9 | 12.6 | 32.8 | 13.36 | 55.3 |
| standard dev | 5.5 | 15.3 | 7.3 | 19.8 | 7.9 | 20.5 | 5.6 | 26.3 |

^aThe highest values of the enrichment factor EF are highlighted in bold ($EF^{1\%}$) and underline ($EF^{10\%}$), respectively, for each DUD target. For comparison, the $EF^{10\%}$ results obtained by HWZ score are multiplied by a factor of 10. ^bEnrichment factor values are from ref 40.

The efficiency metric was computed by using the enrichment factor $EF^{x\%}$ and hit rate $HR^{x\%}$ at 1%, 5%, and 10% for each of the 40 DUD targets.

A variant of the enrichment statistic was developed to avoid the sensitivity of the small changes in ranking. The receiver

operator characteristic (ROC) curve approach has been used extensively in the life sciences and social sciences arenas since its inception.³⁷ For a recent application of the ROC curve in virtual screening, see the work of Tribelleau.^{35a} The ROC curve is a graphical plot of the sensitivity (true positive rate) vs

Table 7. Enrichment Factor at Top 1% and 10% Obtained with HWZ Score and Several Distinct Programs Corresponding to Structural-Based Virtual Screenings^a

| target | HWZ score | | Suflex-dock ^b | | FRED ^b | | FlexX ^b | | ICM ^b | | DOCK ^b | |
|---------------|-----------|-----------|--------------------------|-------------|-------------------|------|--------------------|------|------------------|-------------|-------------------|------|
| | 1% | 10% | 1% | 10% | 1% | 10% | 1% | 10% | 1% | 10% | 1% | 10% |
| ADA | 29.1 | 64 | 7.7 | 48.7 | 5.1 | 12.8 | 5.1 | 33.3 | 0 | 2.6 | 15 | 40 |
| CDK2 | 18.7 | 40 | 6.9 | 44.4 | 18.1 | 31.9 | 11.1 | 29.2 | 13.9 | 38.9 | 10 | 25 |
| DHFR | 29.2 | 89 | 17.6 | 52.9 | 5.8 | 17.6 | 11.9 | 36.8 | 19.0 | 66.8 | 25 | 60 |
| FXA | 33.3 | 68 | 17.1 | 59.6 | 4.1 | 13.7 | 14.4 | 44.5 | 7.5 | 45.2 | 5 | 35 |
| HIVRT | 19.1 | 42 | 18.6 | 27.9 | 18.6 | 32.6 | 0 | 4.6 | 11.6 | 37.2 | 5 | 25 |
| NA | 26.8 | 76 | 22.4 | 67.4 | 0 | 4.1 | 4.1 | 69.4 | 34.7 | 85.7 | 10 | 60 |
| P38 | 24.6 | 51 | 3.7 | 18.1 | 7.9 | 19.6 | 1.1 | 21.6 | 4.6 | 7.5 | 2 | 25 |
| thrombin | 21.2 | 56 | 5.6 | 47.2 | 1.4 | 11.1 | 6.9 | 52.8 | 5.6 | 33.3 | 5 | 35 |
| TK | 19.7 | 49 | 0 | 13.6 | 18.2 | 22.7 | 0 | 13.6 | 0 | 0 | 0 | 25 |
| trypsin | 32.5 | 59 | 18.4 | 81.6 | 2.0 | 26.5 | 0 | 51.0 | 2.0 | 18.4 | 0 | 30 |
| average | 25.4 | 59.4 | 11.8 | 46.1 | 8.1 | 19.3 | 5.5 | 35.7 | 9.9 | 33.6 | 7.7 | 36.0 |
| standard dev. | 5.6 | 15.3 | 7.8 | 21.4 | 7.4 | 9.3 | 5.4 | 19.6 | 10.7 | 27.9 | 7.7 | 13.7 |

^aThe highest values of the enrichment factor EF are highlighted in bold (EF^{1%}) and underline (EF^{10%}), respectively, for each DUD target. For comparison, the EF^{10%} results obtained by HWZ score are multiplied by a factor of 10. ^bEnrichment factor values are from ref 40.

1 – specificity (false positive rate). The sensitivity (Se) and specificity (Sp) are defined as

$$Se = \frac{TP}{TP + FN} \quad (8)$$

$$Sp = \frac{TN}{TN + FP} \quad (9)$$

where TP represents the number of correctly identified actives (true positives), TN, the number of correctly identified inactives (true negatives), FP, the number of inactives incorrectly predicted as actives (false positives), and FN the number of actives incorrectly predicted to be inactive (false negatives).

The area under the ROC curve (AUC) represents another descriptor for virtual screening performance and can be calculated as the sum of all rectangles formed by the sensitivity (Se) and specificity (1 – Sp) values for different thresholds.^{35a} The AUC of a ROC plot gives an objective measure of query performance which is essentially independent of the actual number of positive and negative instances. For the ideal distributions of actives and decoys, an AUC value of 1 would be obtained; completely random distributions would lead to an AUC value of 0.5. Practical virtual screening workflows that perform better than a random discrimination of the actives and decoys retrieve an AUC value between 0.5 and 1, whereas an AUC value lower than 0.5 represents the unfavorable case of a method that has a higher probability to assign higher scores to decoys than to actives. But a rough guide for classifying the accuracy of a screening test is the traditional academic point system known as follows: 0.9 ≤ AUC ≤ 1 is excellent; 0.80 ≤ AUC < 0.9 is good; 0.70 ≤ AUC < 0.8 is fair; 0.50 ≤ AUC < 0.7 is poor; and AUC < 0.5 is a failure.

The numerical results below are reported with the 95% confidence interval.

RESULTS AND DISCUSSION

As noted above, the HWZ score has been calibrated against 16 drug targets corresponding to a total of 2784 active ligands and 6960 training tests (see SI Table S2 concerning the individual numbers for each target), and the finally calibrated parameters a_k , b_k , and c_k are listed in Table 1. As noted above, we also calibrated the parameters a_k , b_k , and c_k against each of the 16 targets and obtained 16 different sets of parameter values. It is

interesting to note (in SI Table S2) that the obtained 16 sets of parameter values are very close to each other, and there is no difference between the finally calibrated parameter values and the corresponding average values. These data (see in SI Table S2) suggest that the optimal values of the HWZ parameters are nearly independent of the target.

As seen in Table 1, we elected to use $N = 3$ in the present study, because the results obtained from using $N = 3$ are good enough based on the calibration against the 16 targets. Below, we first compare the performance of our shape-filtering approach using the calibrated HWZ score in comparison with approaches using the Tanimoto score and other popularly used scoring approaches for their applications to the compounds for the same 40 targets in the DUD database. All of the computational results discussed below for the other approaches (the ROCS and ShaEP programs) were obtained from literature cited.

Concerning the practical application of a given ligand-based virtual screening to each target, there were always multiple active compounds available in the DUD database. The virtual screening was carried out for multiple times, as each active compound had an equal opportunity to serve as the query. The numerical results reported below all refer to the average. To examine the effectiveness of the HWZ scoring function, we have analyzed the results by using four different indicators, including three discussed below and an additional one, i.e. the Güner-Henry score (GH score) metrics (provided in SI Figure S2).³⁸

Area under the ROC Curve (AUC) Values. The performance of our shape-filtering approach was first tested using the Tanimoto scoring function on the 40 targets in the DUD database. As seen in Table 2, based on our shape-filtering approach using the Tanimoto score, the obtained average AUC value, denoted by ⟨AUC⟩, for the 40 targets was 0.70 ± 0.03 . For comparison, the ⟨AUC⟩ values reported in the literature were 0.73 ± 0.06 ^{20a} and 0.69 ± 0.05 ¹⁴ obtained by using the ROCS program^{8c,24} and 0.64 ± 0.05 ¹⁴ by using ShaEP program. The ROCS uses the Combo Scoring function (Shape-Tanimoto and Scaled Color score), whereas the ShaEP uses the Hodgkin²³ similarity index. It is interesting to note that the three scoring functions demonstrated the close overall performance in the tests on the 40 targets based on the AUC metric.

Further, based on our shape-filtering approach using the HWZ scoring function, the average AUC value, denoted by $\langle \text{AUC} \rangle$, for the 40 targets was 0.84 ± 0.02 , demonstrating a “good” virtual screening performance. A detailed analysis of the AUC values obtained for individual targets (Table 3) revealed that the AUC value was never below 0.6 when the HWZ score was used for any target, whereas the AUC was below 0.6 for 9 of the 40 targets ($\sim 23\%$) when the Tanimoto score was used (see Figure 3 and Table 2). Overall, when the HWZ score was used, we obtained $\text{AUC} \geq 0.8$ for 29 targets (72%). In comparison, in the reported use of the ROCS, $\text{AUC} \geq 0.8$ for only 17 targets (42% targets)^{20a} or 12 targets (30%).¹⁴ Further, when the HWZ score was used, we obtained $\text{AUC} \geq 0.6$ for all of the 40 targets (100%). In comparison, in the reported use of the ROCS, $\text{AUC} \geq 0.6$ for only 28 targets (70%)^{20a} or 26 targets (65%).¹⁴ As $\text{AUC} < 0.6$ (cutoff) is considered to be associated with a “poor-fail” screening, the reported screening tests using the ROCS failed for 12 targets (30%)^{20a} or 14 targets (35%),¹⁴ whereas the use of the HWZ score did not fail for any of the 40 targets.

It should also be pointed out that, despite the better performance of the HWZ scoring function for most targets, our virtual screening using the HWZ scoring function had unsatisfactory performance for few targets (exceptions). The worst performance of the virtual screening using the HWZ score was associated with the ER antagonist target, for which $\text{AUC} = 0.6$ using the HWZ score and $\text{AUC} = 0.59$ using the Tanimoto score. In comparison, for the same ER antagonist target, $\text{AUC} = 0.98$ or 0.78 for the reported virtual screening tests using the ROCS, as seen in Table 3. Carefully checking the molecular structures of the active ligands, we noted that these exceptions, including the ER antagonist target, might be associated with some highly flexible structures of the active ligands and the use of different superimposition approaches. For example, many of the ER antagonists include alkyl chains with several rotatable bonds and it is tricky to overlap the highly flexible alkyl chains with other more rigid structures like aromatic rings. Therefore, the worst result of our virtual screening for this particular target is likely attributed to the superimposition approach implemented in the algorithm. Further development of the virtual screening method should be focused on improvement of the superimposition approach.

As seen in Table 3, the virtual screening performance of the ROCS was strongly influenced by the choice of the target. In comparison, the performance of our HWZ score-based virtual screening was least sensitive to the choice of the target.

To further examine the effectiveness of the HWZ scoring function, we have also compared our results with the other published data³⁹ for the same targets in the DUD database, but we have only found nine common targets. Summarized in Table 4 are the results reported for the nine common targets involving five distinct programs/scoring functions, in comparison with the corresponding results obtained from using the HWZ scoring function. As seen in Table 4, the HWZ score provided the highest AUC values for all of the targets, except for DHFR. For DHFR, the best result ($\text{AUC} = 0.95$) is associated with the AutoDoc_{Rigorous} program, but the AutoDoc_{Rigorous} program performed very poorly for the other targets ($\text{AUC} = 0.35\text{--}0.58$), as seen in Table 4. The data in Table 4 suggest that the HWZ scoring function has the overall best performance within the common targets

Table 8. Hit Rates at Top 1%, 5%, and 10% Using Our HWZ Score-Based Method in Comparison with the Corresponding Results Reported by Kirchmair et al. Using the ROCS Program

| target | HR 1% | | HR 5% | | HR 10% | |
|----------------|-----------|-------------------|-----------|-------------------|-----------|-------------------|
| | HWZ score | ROCS ^a | HWZ score | ROCS ^a | HWZ score | ROCS ^a |
| ACE | 47.8 | 70.9 | 35.0 | 41.0 | 31.0 | 47.0 |
| ACHE | 68.9 | 68.2 | 42.5 | 63.0 | 58.2 | 74.0 |
| ADA | 72.2 | 34.2 | 67.6 | 17.5 | 64.0 | 39.0 |
| ALR2 | 40.8 | 21.2 | 34.4 | 15.5 | 48.5 | 31.0 |
| AMPC | 73.1 | 96.0 | 54.9 | 68.0 | 51.5 | 72.0 |
| AR | 62.2 | 64.3 | 36.1 | 47.5 | 50.6 | 51.0 |
| CDK2 | 42.5 | 59.9 | 25.6 | 32.0 | 39.8 | 40.0 |
| COMT | 38.4 | 70.7 | 41.5 | 27.5 | 45.7 | 27.0 |
| COX-1 | 19.2 | 44.2 | 24.1 | 28.5 | 40.5 | 28.0 |
| COX-2 | 14.2 | 57.0 | 20.2 | 85.5 | 72.3 | 87.0 |
| DHFR | 66.4 | 76.1 | 77.5 | 70.0 | 89.0 | 82.0 |
| EGFR | 69.7 | 75.3 | 58.8 | 84.5 | 52.9 | 89.0 |
| ER agonist | 61.6 | 66.5 | 60.5 | 80.5 | 62.1 | 90.0 |
| ER antagonist | 26.1 | 6.6 | 43.0 | 75.0 | 56.1 | 98.0 |
| FGFR1 | 33.8 | 0.0 | 56.1 | 12.0 | 54.7 | 20.0 |
| FXA | 37.3 | 4.8 | 71.2 | 5.0 | 68.2 | 8.0 |
| GART | 12.3 | 0.0 | 64.4 | 19.5 | 81.0 | 57.0 |
| GPB | 41.2 | 85.6 | 39.1 | 73.0 | 52.4 | 81.0 |
| GR | 25.1 | 17.2 | 39.5 | 26.0 | 45.1 | 57.0 |
| HIVPR | 28.1 | 5.8 | 37.5 | 11.5 | 56.2 | 15.0 |
| HIVRT | 42.8 | 47.2 | 27.1 | 23.0 | 41.5 | 25.0 |
| HMGA | 51.0 | 61.7 | 84.0 | 78.0 | 79.2 | 83.0 |
| HSP90 | 77.8 | 86.5 | 52.7 | 46.0 | 57.4 | 46.0 |
| INHA | 13.4 | 64.1 | 33.3 | 49.5 | 47.3 | 51.0 |
| MR | 65.9 | 75.0 | 75.5 | 81.5 | 84.3 | 80.0 |
| NA | 70.3 | 84.7 | 65.5 | 92.5 | 76.3 | 96.0 |
| P38 | 36.8 | 15.3 | 53.4 | 14.0 | 51.2 | 20.0 |
| PARP | 78.1 | 7.1 | 71.5 | 15.5 | 66.1 | 37.0 |
| PDE5 | 29.4 | 21.3 | 55.7 | 20.0 | 55.6 | 24.0 |
| PDGFRB | 25.8 | 16.0 | 35.8 | 8.5 | 44.3 | 11.0 |
| PNP | 71.3 | 48.7 | 74.0 | 84.5 | 73.7 | 93.0 |
| PPAR γ | 41.0 | 21.6 | 78.5 | 79.0 | 65.3 | 83.0 |
| PR | 67.9 | 34.7 | 62.2 | 15.0 | 71.0 | 26.0 |
| RXR α | 87.2 | 62.4 | 92.5 | 86.0 | 92.0 | 86.0 |
| SAHH | 65.0 | 64.5 | 80.5 | 73.5 | 88.1 | 94.0 |
| SRC | 29.3 | 3.1 | 48.6 | 8.0 | 49.8 | 10.0 |
| thrombin | 21.2 | 1.8 | 36.5 | 5.5 | 55.7 | 7.0 |
| TK | 48.6 | 33.8 | 43.5 | 23.0 | 49.1 | 60.0 |
| trypsin | 32.5 | 0.0 | 63.6 | 0.0 | 59.2 | 28.0 |
| VEGFR2 | 14.5 | 0.0 | 24.9 | 1.5 | 39.1 | 4.0 |
| average | 46.3 | 41.9 | 52.2 | 42.2 | 59.2 | 51.4 |
| 95% confidence | 6.7 | 9.5 | 5.9 | 9.5 | 4.7 | 9.4 |

^aData from ref 20a.

available for comparison. The highest average AUC value, 0.83 ± 0.05 , is associated with the HWZ scoring function. On the other hand, we are reluctant to make a final conclusion on this simply based on the data in Table 4 due to the very limited number of available common targets for comparison.

Enrichments Factor. The results of our screening tests were further analyzed using the enrichment factor (EF). The EF values at 1% and 5% of the data set describe the early enrichment, whereas the EF value at 10% represents the late-stage

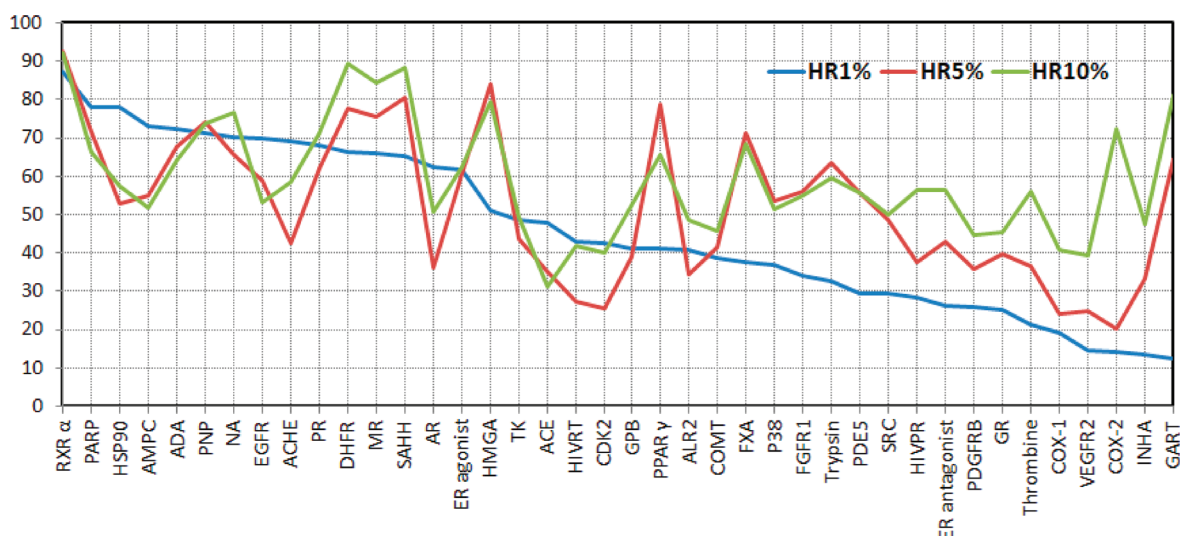


Figure 5. Hit rate (HR) values at 1%, 5%, and 10% obtained from the HWZ score-based virtual screening. For clarity, the hit rate was sorted from the highest HR^{1%} value to the lowest one.

database screening. The EF values are summarized in Table 5 and depicted in Figure 4 for the 40 targets. As seen in Table 5, our HWZ score-based virtual screening led to an average EF^{1%} value of 23.7 ± 2.6 , compared to the reported average EF^{1%} value^{20a} of 19.4 ± 4.0 obtained by using the ROCS program.

In addition, the data in Figure 4 and Table 5 indicate that our HWZ score-based virtual screening never completely failed as no target was associated with EF^{1%} = 0 within the 40 targets, whereas the reported virtual screening^{20a} using the ROCS could not identify any active ligand for four targets (GART, Trypsin, FGFR1, and VEGFR2).

Concerning the average enrichment at top 5% for the 40 targets, our HWZ score-based virtual screening led to an average EF^{5%} value of 10.4 ± 1.2 , compared to the reported average EF^{5%} value of 8.4 ± 1.9 obtained by using ROCS.^{20a} For the late-stage screening database screening enrichment factor (EF^{10%}) for the 40 targets, our HWZ score-based virtual screening led to an average EF^{10%} value of 5.9 ± 0.5 , compared to the reported average EF^{10%} value^{20a} of 5.1 ± 0.9 obtained by using ROCS.

Concerning the EF^{10%} values for individual targets, the data in Table 5 indicate that the EF^{10%} values in our HWZ score-based virtual screening range from 3.1 to 9.2, whereas the reported EF^{10%} values associated with ROCS range from 0.4 to 9.8. So, our HWZ score-based virtual screening was less sensitive to the choice of target. Overall, our HWZ score-based virtual screening demonstrated an improved performance.

We also tried to compare the EF values from the HWZ score-based virtual screening with those from other virtual screening tests for the same targets in the DUD database, but we have only found 10 common targets (see Table 6 for comparison with the ligand-based methods and Table 7 for comparison with the structure-based methods). As seen in Tables 6 and 7, the obtained EF^{1%} and EF^{10%} values associated with the HWZ score are least-sensitive to the target, whereas the data obtained from the other methods are rather sensitive to the target and, therefore, the relative EF^{1%} or EF^{10%} values are dependent on the target when different methods are compared. In comparison with the ligand-based methods, the largest EF^{1%} value is associated with the HWZ score for 8 targets, and the largest EF^{10%} value is associated with the HWZ score for 6 targets, as seen in Table 6. In comparison with the structure-based

methods, the largest EF^{1%} value is associated with the HWZ score for 9 targets, and the largest EF^{10%} value is associated with the HWZ score for 7 targets, as seen in Table 7. Overall, the largest average EF^{1%} and EF^{10%} values are all associated with the HWZ score within the 10 common targets available for comparison. Nevertheless, we are reluctant to make a final conclusion on this simply based on the data in Tables 6 and 7 due to the very limited number of available common targets for comparison.

Hit Rate. Summarized in Table 8 and depicted in Figure 5 are the hit rates obtained from our HWZ score-based virtual screening and the ROCS-based virtual screening reported in literature for the 40 targets in the DUD database. As seen in Table 8, the average HR value at top 1% (HR^{1%}) was $46.3\% \pm 6.6\%$ for our HWZ score-based virtual screening and $41.9\% \pm 9.5\%$ for the ROCS-based virtual screening reported by Kirchmair et al.^{20a} The average HR^{5%} value was $52.2\% \pm 5.9\%$ for our HWZ score-based virtual screening and $42.2\% \pm 9.5\%$ for the ROCS-based virtual screening reported by Kirchmair et al.^{20a} The average HR^{10%} value was $59.1\% \pm 4.7\%$ for our HWZ score-based virtual screening and $51.4\% \pm 9.4\%$ for the ROCS-based virtual screening reported by Kirchmair et al.^{20a} All of these HR values indicate that our HWZ score-based virtual screening demonstrated an improved performance.

CONCLUSION

In the present report, we have developed and implemented a robust new scoring function, i.e. the HWZ score, for ligand-based (shape-filtering) virtual screening method. Compared to other popularly used shape-filtering virtual screening approaches (using different scoring functions) examined for their applications to the compounds for the same 40 protein targets in the DUD database, our HWZ score-based virtual screening approach led to an improved overall performance based on the obtained AUC, enrichment factor, and hit rate values. In addition, the performance of the HWZ score-based virtual screening approach was less sensitive to the choice of the target. The generation of a novel and robust scoring function is not only useful for ligand-based virtual screening algorithms, but it may also open the door for the ranking of docking results.

■ ASSOCIATED CONTENT

■ Supporting Information

Detailed information about the calibration of the HWZ scoring function. This material is available free of charge via the Internet at <http://pubs.acs.org>.

■ AUTHOR INFORMATION

Corresponding Author

*Tel.: 859-323-3943. Fax: 859-323-3575. E-mail: zhan@uky.edu.

Author Contributions

[§]These authors contributed equally to this work.

Notes

The authors declare no competing financial interest.

■ ACKNOWLEDGMENTS

This work was supported in part by the NIH (grant RC1MH088480 to Zhan). We gratefully acknowledge Professor Emeritus Dan Vasilescu (University of Nice Sophia-Antipolis, France) and Professor Ramaswamy H. Sarma (University at Albany) for the long discussions concerning the use of some mathematic models. The authors also acknowledge the Computer Center at University of Kentucky for supercomputing time on a Dell Supercomputer Cluster consisting of 388 nodes or 4816 processors.

■ REFERENCES

- (1) (a) John, S.; Thangapandian, S.; Sakikah, S.; Lee, K. W. Discovery of potential pancreatic cholesterol esterase inhibitors using pharmacophore modelling, virtual screening, and optimization studies. *J. Enzyme Inhib. Med. Chem.* **2011**, *26* (4), 535–545. (b) Bi, J.; Yang, H.; Yan, H.; Song, R.; Fan, J. Knowledge-based virtual screening of HLA-A*0201-restricted CD8(+) T-cell epitope peptides from herpes simplex virus genome. *J. Theor. Biol.* **2011**, *281* (1), 133–139. (c) Akula, N.; Zheng, H.; Han, F. Q.; Wang, N. Discovery of novel SecA inhibitors of *Candidatus Liberibacter asiaticus* by structure based design. *Bioorg. Med. Chem. Lett.* **2011**, *21* (14), 4183–4188.
- (2) (a) Rai, B. K.; Tawa, G. J.; Katz, A. H.; Humblet, C. Modeling G protein-coupled receptors for structure-based drug discovery using low-frequency normal modes for refinement of homology models: Application to H3 antagonists. *Proteins-Struct. Funct. Bioinf.* **2010**, *78* (2), 457–473. (b) Palczewski, K.; Kumasaka, T.; Hori, T.; Behnke, C. A.; Motoshima, H.; Fox, B. A.; Le Trong, I.; Teller, D. C.; Okada, T.; Stenkamp, R. E.; Yamamoto, M.; Miyano, M. Crystal structure of rhodopsin: A G protein-coupled receptor. *Science* **2000**, *289* (5480), 739–745. (c) Stevens, R. C.; Cherezov, V.; Rosenbaum, D. M.; Hanson, M. A.; Rasmussen, S. G. F.; Thian, F. S.; Kobilka, T. S.; Choi, H. J.; Kuhn, P.; Weiss, W. I.; Kobilka, B. K. High-resolution crystal structure of an engineered human beta(2)-adrenergic G protein-coupled receptor. *Science* **2007**, *318* (5854), 1258–1265. (d) Stevens, R. C.; Jaakola, V. P.; Griffith, M. T.; Hanson, M. A.; Cherezov, V.; Chien, E. Y. T.; Lane, J. R.; Ijzerman, A. P. The 2.6 Å Crystal Structure of a Human A(2A) Adenosine Receptor Bound to an Antagonist. *Science* **2008**, *322* (5905), 1211–1217. (e) Xu, Y.; Kim, D.; Xu, D.; Guo, J. T.; Ellrott, K. PROSPECT II: protein structure prediction program for genome-scale applications. *Protein Eng.* **2003**, *16* (9), 641–650. (f) Honig, B.; Petrey, D.; Xiang, Z. X.; Tang, C. L.; Xie, L.; Gimpelev, M.; Mitros, T.; Soto, C. S.; Goldsmith-Fischman, S.; Kernysky, A.; Schlessinger, A.; Koh, I. Y. Y.; Alexov, E. Using multiple structure alignments, fast model building, and energetic analysis in fold recognition and homology modeling. *Proteins-Struct. Funct. Genetics* **2003**, *53* (6), 430–435. (g) Simons, K. T.; Kooperberg, C.; Huang, E.; Baker, D. Assembly of protein tertiary structures from fragments with similar local sequences using simulated annealing and Bayesian scoring functions. *J. Mol. Biol.* **1997**, *268* (1), 209–225.
- (3) Jegerschold, C.; Paweizik, S. C.; Purhonen, P.; Bhakat, P.; Gheorghe, K. R.; Gyobu, N.; Mitsuoka, K.; Morgenstern, R.; Jakobsson, P. J.; Hebert, H. Structural basis for induced formation of the inflammatory mediator prostaglandin E-2. *Proc. Natl. Acad. Sci. U.S.A.* **2008**, *105* (32), 11110–11115.
- (4) Tresadern, G.; Bemporad, D.; Howe, T. A comparison of ligand based virtual screening methods and application to corticotropin releasing factor 1 receptor. *J. Mol. Graphics Modell.* **2009**, *27* (8), 860–870.
- (5) (a) Saeh, J. C.; Lyne, P. D.; Takasaki, B. K.; Cosgrove, D. A. Lead hopping using SVM and 3D pharmacophore fingerprints. *J. Chem. Inf. Model.* **2005**, *45* (4), 1122–1133. (b) von Korff, M.; Freyss, J.; Sander, T. Flexophore, a new versatile 3D pharmacophore descriptor that considers molecular flexibility. *J. Chem. Inf. Model.* **2008**, *48* (4), 797–810.
- (6) Ballester, P. J.; Finn, P. W.; Richards, W. G. Ultrafast shape recognition: Evaluating a new ligand-based virtual screening technology. *J. Mol. Graphics Modell.* **2009**, *27* (7), 836–845.
- (7) (a) Lemmen, C.; Lengauer, T. Computational methods for the structural alignment of molecules. *J. Comput.-Aided Mol. Des.* **2000**, *14* (3), 215–232. (b) Maldonado, A. G.; Doucet, J. P.; Petitjean, M.; Fan, B. T. Molecular similarity and diversity in chemoinformatics: From theory to applications. *Mol. Diversity* **2006**, *10* (1), 39–79. (c) Melani, F.; Gratteri, P.; Adamo, M.; Bonaccini, C. Field interaction and geometrical overlap: A new simplex and experimental design based computational procedure for superposing small ligand molecules. *J. Med. Chem.* **2003**, *46* (8), 1359–1371.
- (8) (a) Grant, J. A.; Gallardo, M. A.; Pickup, B. T. A fast method of molecular shape comparison: A simple application of a Gaussian description of molecular shape. *J. Comput. Chem.* **1996**, *17* (14), 1653–1666. (b) Nicholls, A.; Grant, J. A. Molecular shape and electrostatics in the encoding of relevant chemical information. *J. Comput.-Aided Mol. Des.* **2005**, *19* (9–10), 661–686. (c) Rush, T. S.; Grant, J. A.; Mosyak, L.; Nicholls, A. A shape-based 3-D scaffold hopping method and its application to a bacterial protein-protein interaction. *J. Med. Chem.* **2005**, *48* (5), 1489–1495.
- (9) Wolber, G.; Kirchmair, J.; Distinto, S.; Markt, P.; Schuster, D.; Spitzer, G. M.; Liedl, K. R. How To Optimize Shape-Based Virtual Screening: Choosing the Right Query and Including Chemical Information. *J. Chem. Inf. Model.* **2009**, *49* (3), 678–692.
- (10) Hawkins, P. C. D.; Skillman, A. G.; Nicholls, A. Comparison of shape-matching and docking as virtual screening tools. *J. Med. Chem.* **2007**, *50* (1), 74–82.
- (11) Singh, J.; Chuaqui, C. E.; Boriack-Sjodin, P. A.; Lee, W. C.; Pontz, T.; Corbley, M. J.; Cheung, H. K.; Arduini, R. M.; Mead, J. N.; Newman, M. N.; Papadatos, J. L.; Bowes, S.; Josiah, S.; Ling, L. E. Successful shape-based virtual screening: The discovery of a potent inhibitor of the type I TGF beta receptor kinase (T beta RI). *Bioorg. Med. Chem. Lett.* **2003**, *13* (24), 4355–4359.
- (12) Livingstone, D. J.; Clark, T.; Ford, M. G.; Hudson, B. D.; Whitley, D. C. QSAR studies using the parashift system. *SAR QSAR Environ. Res.* **2008**, *19* (3–4), 285–302.
- (13) (a) Ritchie, D. W.; Kemp, G. J. L. Protein docking using spherical polar Fourier correlations. *Proteins-Struct. Funct. Genetics* **2000**, *39* (2), 178–194. (b) Perez-Nueno, V. I.; Ritchie, D. W.; Borrell, J. I.; Teixido, J. Clustering and Classifying Diverse HIV Entry Inhibitors Using a Novel Consensus Shape-Based Virtual Screening Approach: Further Evidence for Multiple Binding Sites within the CCR5 Extracellular Pocket. *J. Chem. Inf. Model.* **2008**, *48* (11), 2146–2165.
- (14) Vainio, M. J.; Puranen, J. S.; Johnson, M. S. ShaEP: Molecular Overlay Based on Shape and Electrostatic Potential. *J. Chem. Inf. Model.* **2009**, *49* (2), 492–502.
- (15) Ballester, P. J.; Richards, W. G. Ultrafast shape recognition to search compound databases for similar molecular shapes. *J. Comput. Chem.* **2007**, *28* (10), 1711–1723.
- (16) Putta, S.; Beroza, P. Shapes of things: Computer modeling of molecular shape in drug discovery. *Curr. Top. Med. Chem.* **2007**, *7* (15), 1514–1524.

- (17) Kirchmair, J.; Markt, P.; Distinto, S.; Wolber, G.; Langer, T. Evaluation of the performance of 3D virtual screening protocols: RMSD comparisons, enrichment assessments, and decoy selection - What can we learn from earlier mistakes? *J. Comput.-Aided Mol. Des.* **2008**, *22* (3–4), 213–228.
- (18) (a) Lyne, P. D. Structure-based virtual screening: an overview. *Drug Discovery Today* **2002**, *7* (20), 1047–1055. (b) Shoichet, B. K.; McGovern, S. L.; Wei, B. Q.; Irwin, J. J. Lead discovery using molecular docking. *Curr. Opin. Chem. Biol.* **2002**, *6* (4), 439–446. (c) Doman, T. N.; McGovern, S. L.; Witherbee, B. J.; Kasten, T. P.; Kurumbail, R.; Stallings, W. C.; Connolly, D. T.; Shoichet, B. K. Molecular docking and high-throughput screening for novel inhibitors of protein tyrosine phosphatase-1B. *J. Med. Chem.* **2002**, *45* (11), 2213–2221.
- (19) Langer, T.; Krovat, E. M. Chemical feature-based pharmacophores and virtual library screening for discovery of new leads. *Curr. Opin. Drug Discovery Dev.* **2003**, *6* (3), 370–376.
- (20) (a) Kirchmair, J.; Distinto, S.; Markt, P.; Schuster, D.; Spitzer, G. M.; Liedl, K. R.; Wolber, G. How To Optimize Shape-Based Virtual Screening: Choosing the Right Query and Including Chemical Information. *J. Chem. Inf. Model.* **2009**, *49* (3), 678–692. (b) Sastry, G. M.; Dixon, S. L.; Sherman, W. Rapid Shape-Based Ligand Alignment and Virtual Screening Method Based on Atom/Feature-Pair Similarities and Volume Overlap Scoring. *J. Chem. Inf. Model.* **2011**, *51* (10), 2455–2466.
- (21) Jahn, A.; Hinselmann, G.; Nikolas Fechner, N.; Zell, A. Optimal assignment methods for ligand-based virtual screening. *J. Cheminf.* **2009**, *1* (14), 1–23.
- (22) Rogers, D. J.; Tanimoto, T. T. A computer program for classifying plants. *American Association for the Advancement of Science. Science* **1960**, *132*, 1115–18.
- (23) Hodgkin, E. E.; Richards, W. G. Molecular Similarity Based on Electrostatic Potential and Electric-Field. *Int. J. Quantum Chem.* **1987**, 105–110.
- (24) ROCS; OpenEye Scientific Software, Inc., Santa Fe, NM, USA, 2007; www.eyesopen.com.
- (25) (a) Vand, V. A Simplified Method of Steepest Descents. *Acta Crystallogr.* **1951**, *4* (3), 285–286. (b) Steinmet, H. I. Using Method of Steepest Descent. *Ind. Eng. Chem.* **1966**, *58* (1), 33. (c) Chapman, P. B. Method of Steepest Descent. *Can. Math. Bull.* **1967**, *10* (1), 133–8.
- (26) (a) Coutsiar, E. A.; Seok, C.; Dill, K. A. Using quaternions to calculate RMSD. *J. Comput. Chem.* **2004**, *25* (15), 1849–1857. (b) Coutsiar, E. A.; Seok, C.; Dill, K. A. Rotational superposition and least squares: The SVD and quaternions approaches yield identical results. Reply to the preceding comment by G. Kneller. *J. Comput. Chem.* **2005**, *26* (15), 1663–1665. (c) Karney, C. F. F. Quaternions in molecular modeling. *J. Mol. Graphics Modell.* **2007**, *25* (5), 595–604.
- (27) Hamza, A.; Zhao, X.; Tong, M.; Tai, H. H.; Zhan, C. G. Novel human mPGES-1 inhibitors identified through structure-based virtual screening. *Bioorg. Med. Chem.* **2011**.
- (28) Grant, J. A.; Pickup, B. T. A Gaussian Description of Molecular Shape. *J. Phys. Chem.* **1995**, *99* (11), 3503–3510.
- (29) Huang, N.; Shoichet, B. K.; Irwin, J. J. Benchmarking sets for molecular docking. *J. Med. Chem.* **2006**, *49* (23), 6789–6801.
- (30) Cross, J. B.; Thompson, D. C.; Rai, B. K.; Baber, J. C.; Fan, K. Y.; Hu, Y. B.; Humblet, C. Comparison of Several Molecular Docking Programs: Pose Prediction and Virtual Screening Accuracy. *J. Chem. Inf. Model.* **2009**, *49* (6), 1455–1474.
- (31) Nicholls, A. What do we know and when do we know it? *J. Comput.-Aided Mol. Des.* **2008**, *22* (3–4), 239–255.
- (32) Omega-2.2; Open Eye Scientific Software, 2007; www.eyesopen.com.
- (33) Bostrom, J.; Greenwood, J. R.; Gottfries, J. Assessing the performance of OMEGA with respect to retrieving bioactive conformations. *J. Mol. Graphics Modell.* **2003**, *21* (5), 449–462.
- (34) (a) Jacobsson, M.; Liden, P.; Stjernschantz, E.; Bostrom, H.; Norinder, U. Improving structure-based virtual screening by multivariate analysis of scoring data. *J. Med. Chem.* **2003**, *46* (26), 5781–5789. (b) Hecker, E. A.; Duraiswami, C.; Andrea, T. A.; Diller, D. J. Use of catalyst pharmacophore models for screening of large combinatorial libraries. *J. Chem. Inf. Comput. Sci.* **2002**, *42* (5), 1204–1211. (c) Diller, D. J.; Li, R. X. Kinases, homology models, and high throughput docking. *J. Med. Chem.* **2003**, *46* (22), 4638–4647.
- (35) (a) Triballeau, N.; Acher, F.; Brabet, I.; Pin, J. P.; Bertrand, H. O. Virtual screening workflow development guided by the “receiver operating characteristic” curve approach. Application to high-throughput docking on metabotropic glutamate receptor subtype 4. *J. Med. Chem.* **2005**, *48* (7), 2534–2547. (b) Truchon, J. F.; Bayly, C. I. Evaluating virtual screening methods: Good and bad metrics for the “early recognition” problem. *J. Chem. Inf. Model.* **2007**, *47* (2), 488–508.
- (36) Bissantz, C.; Folkers, G.; Rognan, D. Protein-based virtual screening of chemical databases. 1. Evaluation of different docking/scoring combinations. *J. Med. Chem.* **2000**, *43* (25), 4759–4767.
- (37) (a) Hanley, J. A.; McNeil, B. J. The Meaning and Use of the Area under a Receiver Operating Characteristic (ROC) Curve. *Radiology* **1982**, *143* (1), 29–36. (b) Baldi, P.; Brunak, S.; Chauvin, Y.; Andersen, C. A. F.; Nielsen, H. Assessing the accuracy of prediction algorithms for classification: an overview. *Bioinformatics* **2000**, *16* (5), 412–424.
- (38) Fisher, L. S.; Guner, O. F. Seeking novel leads through structure-based pharmacophore design. *J. Braz. Chem. Soc.* **2002**, *13* (6), 777–787.
- (39) Durrant, J. D.; McCammon, J. A. NNScore 2.0: A Neural-Network Receptor-Ligand Scoring Function. *J. Chem. Inf. Model.* **2011**, *51* (11), 2897–2903.
- (40) Giganti, D.; Guillemin, H.; Spadoni, J.-L.; Nilges, M.; Zagury, J.-F.; Montes, M. Comparative Evaluation of 3D Virtual Ligand Screening Methods: Impact of the Molecular Alignment on Enrichment. *J. Chem. Inf. Model.* **2010**, *50* (6), 992–1004.